Anal. Bioanal. Electrochem., Vol. 10, No. 2, 2018, 161-174

Analytical & Bioanalytical Electrochemistry

Full Paper

The Role of Grain Refinement in Micro-scales on Passive and Semiconducting Properties of 304 Stainless Steel in an Acidic Solution

Fathallah Qods,[1] Saber Maryanaji[1,*] and Arash Fattah-alhosseini[2]

[1]*Metallurgy and Materials Engineering Department, Engineering Faculty, Semnan University, Semnan 19111-35131, Iran*
[2]*Department of Materials Engineering, Bu-Ali Sina University, Hamedan 65178-38695, Iran*

*Corresponding Author, Tel.: +98 2333321006; Fax: +98 2333321005
E-Mail: saber7maryanaji@gmail.com

Received: 7 August 2017 / Received in revised form: 30 November 2017 / Accepted: 19 January 2018 / Published online: 28 February 2018

Abstract- In this research, grain refinement process of AISI 304 stainless steel (304 SS) was successfully performed by an advanced thermomechanical operation. Then, the role of grain refinement on the electrochemical response of 304 SS in an acidic solution (0.1 M HNO_3 solution) was investigated. Microstructural observations depicted that thermomechanical operation resulted in reduction in the grain size from about 37 µm to about 380 nm by a factor of ~100. All the electrochemical experiments concerning the passive and semiconducting properties evaluated by potentiodynamic polarization (PDP), electrochemical impedance spectroscopy (EIS) and Mott–Schottky (M–S) measurements. PDP and EIS plots revealed that grain refinement led to superior conditions for forming the passive layers. M–S tests showed that grain-refining process cannot change the semiconductor properties (n- and p-type semiconductors) of the passive layers. Moreover, M–S tests depicted that the calculated acceptor and donor densities (N_A and N_D) declined with grain refinement. These responses were consistent with the observations of the PDP and EIS tests, evidencing that the passive response enhanced with decreasing the grain size. In conclusion, all the electrochemical experiments depicted that the grain refinement in micro-scales can significantly enhance the passive and semiconducting properties of 304 SS by creation of more stable and compact passive layer.

Keywords- Stainless steel, Thermomechanical operation, Polarization, Mott–Schottky analysis

1. INTRODUCTION

Grain refinement implemented on stainless steel is of a great significance [1,2]. This process affects stainless steel strength and ductility considerably and therefore has received many scientists attention to apply procedures like sever plastic deformation, thermomechanical methods and shot pinning, in order to fabricate steels with fine-grained (FG) structures [3–7]. The possibility of martensitic-plastic transformation at low temperatures in austenitic stainless steel series creates high potential to reach finer grain structures and in turn an attractive field for researchers to investigate the relation of material properties with its grain size [8–12].

Grain refinement can possess different effects on corrosion resistance of an alloy. Therefore, to apperceive the influence of grain refinement on corrosion response, it is necessary to investigate researcher's different surveys in this field. The following examples are presented to elucidate the controversy and complexity of this matter. Di Schino and Kenny [13] performed an experiment on a high nitrogen-low nickel austenitic stainless steel in the 5% wt. H_2SO_4 solution. They recorded the increase of corrosion rate as a result of the reduction in grain size. The investigation by Wu et al. [14] shows that active dissolution of Fe-Ni-Cr steel in solution consisting of 0.05 M H_2SO_4+0.25 M Na_2SO_4 increases as a result of grain refinement. However, on the basis of the investigation conducted by Jinlong and Hongyun, FG 304 stainless steel in comparison with its coarse-grained (CG) counterpart in a borate buffer solution with and without chloride (Cl^-), showed higher corrosion resistance [15]. In addition, Zheng et al. showed that for 304 stainless steel in 0.5 M H_2SO_4 solution grain refining resulted in the improvement of corrosion resistance [16].

Over the last decades, researches concentrating on the electrical properties (particularly semiconducting properties) of passive layer formed on stainless steel surfaces have made an important contribution to comprehend the corrosion behavior of these alloys. In addition to semiconducting properties of passive layer, the influence of alloy microstructure on corrosion behavior is of great importance [17]. Accordingly, the main objective of this work is to investigate the role of grain refinement on the corrosion behavior of 304 SS in 0.1 M HNO_3 solution by electrochemical techniques including OCP, PDP, EIS measurements and also M–S analysis.

2. MATERIALS AND EXPERIMENTAL PROCEDURES

2.1. Samples processing

Table1 shows the chemical composition of 304 SS defined by quantometery analysis. The specimens were prepared with length of 60 mm, width of 40 mm, and thickness of 5 mm. For implementing the rolling experiment, a two-high rolling mill (under oil lubrication) was utilized.

Table 1. Chemical composition of AISI 304 austenitic stainless steel

	Cr	Ni	Mn	Si	C	P	S	Fe
AISI 304 / wt%	18.10	8.24	1.95	0.85	0.07	0.02	0.02	Bal

Schematic of the used thermomechanical treatment to obtain FG 304 SS is available in Fig. 1. According to Fig. 1, in order to perform austenite to martensite transformation the cold rolling was performed down to 90% thickness reduction and at the temperature of -15 °C. The reverse transformation of martensite to austenite was performed by heat treatment of worked sample at 800 °C and for 120 s.

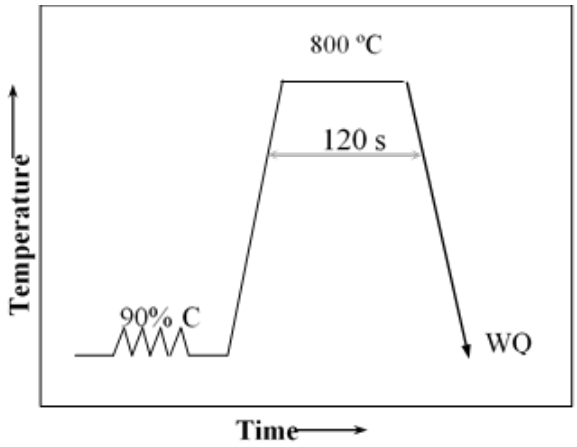

Fig. 1. Schematic of the thermomechanical treatment to obtain FG 304 SS

2.2. Scanning electron microscope (SEM) observations

Surface morphology of CG was examined by optical microscopy and that of FG specimen was examined under a TESCAN SEM. For this purpose, the specimens were polished and then electro-etched. The exact details of electro-etching process are published elsewhere [17,18].

2.3. Electrochemical tests

Both CG and FG specimens were ground to 2000 grit and cleaned by deionized water prior to tests. The exact details of three-electrode flat cell and μAutolab system are published elsewhere [17,18]. Prior to electrochemical experiments, working electrodes (CG and FG specimens) were immersed at open-circuit potential (OCP) conditions for 1800 seconds in 0.1 M HNO3 solution. The electrochemical experiments were carried out in the following progression:

(a) PDP curves were measured starting from –0.25 V (*vs.* E_{corr}) to 1.0 VAg/AgCl (scan rate=0.166 mV/s (ASTM G5-14)).
(b) M–S test was carried out in the cathodic direction (frequency=1 kHz and step potential = 25 mV)
(c) EIS tests were run at OCP conditions with the scanned frequency range from 0.01 Hz to 100 kHz (excitation potential (peak to peak)=10 mV). The other details of M–S analysis and EIS test are published elsewhere [17,18].

3. RESULTS AND DISCUSSION

3.1. SEM observations

The microstructure of both CG and FG specimens is shown in Fig. 2. It is depicted that thermo-mechanical treatment leads to reduction of 304 SS grain size.

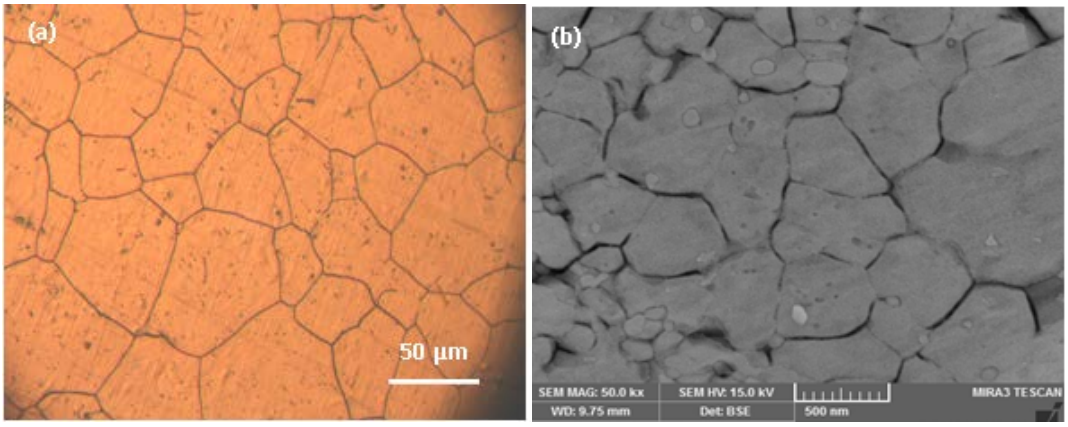

Fig. 2. SEM micrographs of (a) CG and (b) FG specimens

As seen in Fig. 2, the average grain size of CG specimen was about 37 µm in Fig. 2a. After thermomechanical treatment, FG specimen with the average size of 380 nm is acquired in Fig. 2b. Actually, the thermomechanical treatment has been used to fine grain size; on average reduce to 100 times smaller in size.

3.2. OCP tests

The illustration of OCP curves of the CG and FG specimens in 0.1 M HNO3 electrolyte is available in Fig. 3. As can be found in Fig. 3, for both samples, there is an analogous tendency to increase the potential towards positive values during the test time. Such a trend can be attributed to the passive layer formation happening continuously on the surface [18].

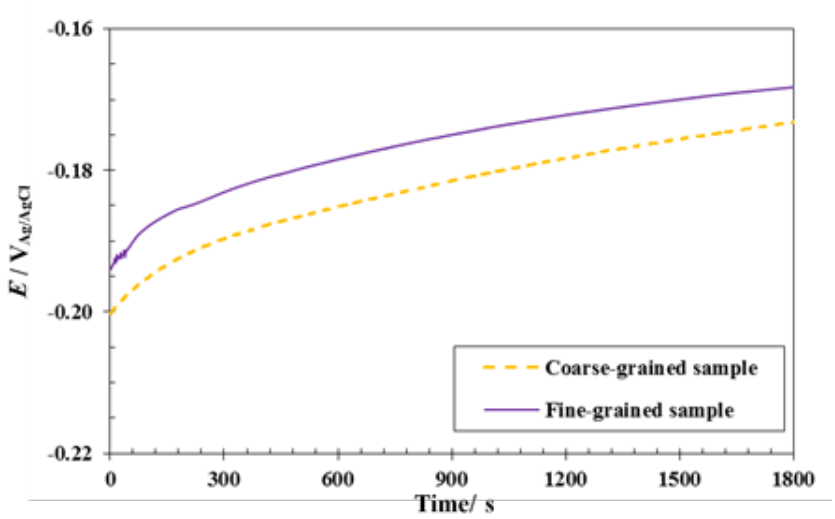

Fig. 3. OCP plots of CG and FG specimens

Also, Fig. 3 demonstrates 1200 seconds as a needed duration to have steady state condition for electrochemical tests run. Completing 1200 seconds with respect to the dominant steady state conditions, the potential slightly changes as the time passes. Then, within a few minutes, especially in oxidizing environments such as HNO_3 solutions, and here in acidic electrolyte the layer of Cr rich oxyhydroxide forms rapidly and as a consequence the potential of stainless steel becomes stable. Steady state conditions within a short while has been also achieved by other researchers. The reports of Wang and Turner [19], Zheng et al. [20] and Cheng et al. [21], define the stable conditions after completing 300 seconds, 600 seconds and 1500 seconds, respectively. Also, Yang et al. [22], Wang et al. [23] and Moura et al. [24] mentioned 1800 seconds for the OCP stabilization. As it can be comprehended, despite of the growing OCP values towards the more positive values for both specimens within duration, FG specimen plot represents more positive values during specific periods in comparison to its CG counterpart. Thus, it can be concluded that in equal exposure to the electrolyte, the passivity in FG sample develops faster than CG one. That is to say, there is a more stable protective passive film on the FG specimen's surface comparing to its CG counterpart. Similar reports are established by Zheng et al. [16] about the 304 stainless steel with nanocrystalline structure produced through equal channel angular pressing. Also, similar conclusions are found in nano-structural layer on the 316L stainless steel fabricate through cavitation-annealing process by Kwok et al. [25].

3.3. PDP measurements

The PDP plots of both CG and FG specimens in the test electrolyte are presented in Fig. 4. Paying attention to the picture, with the smooth and linear change in the applied current around the corrosion potential (E_{corr}), curves with similar shapes are detectable for both samples. Here, cathodic and anodic Tafel behavior is clarified. According to the obtained

polarization curves, thermomechanical operation has lowered passive current density. Also a notable passive current density reduction in the low passive potential area can be observed. Moreover, corrosion current density in FG specimens has been reduced in comparison with the CG ones. According to Fig. 4, two stages of the passive process can be distinguished in the curves. The low potential passive region ranges from about −0.3 to 0.4 $V_{Ag/AgCl}$. In other region, the comparatively slow increase of the current density in the potential range 0.4–0.9 $V_{Ag/AgCl}$ can be connected to the formation of high valence Cr in the oxide film prior to transpassive dissolution [26]. The steeper increase in the range 0.9 to 1.0 $V_{Ag/AgCl}$ is most probably related to the onset of the transpassive dissolution.

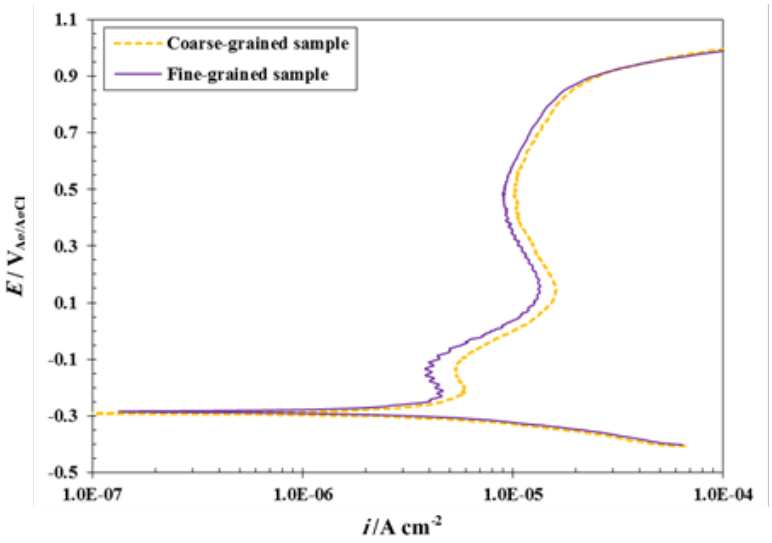

Fig. 4. PDP curves of CG and FG specimens in 0.1 M HNO_3 solution

Considering Fig. 4, more positive values of corrosion potential are related to the samples with fine-grain microstructure. This is in absolute consistent with the OCP figures exhibited in Fig. 3. Since the values of E_{corr} are ascertained from PDP plots, they differ from the OCP values. The aforesaid discrepancy is connected to the partial reduction of metal ions in the passive layer after the application of cathodic polarization while PDP measurements. In addition, potential increase changes the passive layer chemical composition and microstructure. Hence, the values of E_{corr} alter to more negative direction during PDP tests compared to the OCP values gained from Fig. 3 [27].

3.4. M–S analysis

In general, oxide layers without imperfections in the crystalline structures are stoichiometric provided and propounded as insulators. However, point defects existence in the passive layers is the reason of their extrinsic semiconducting behavior in aqueous electrolytes [28,29]. Generally, point defects are described as cation interstitials, and

vacancies of cation and oxygen. Here, vacancies of cation are electron acceptors and define the barrier layer as the p-type semiconductor in doping. On the other hand, metal interstitials and vacancies of oxygen are electron donors and therefore, n-type doping semiconductors [28–31]. Eq. (1) and (2) explain the M–S equations for n- and p-type semiconductor, respectively [28–38]:

$$\frac{1}{C^2} = -\frac{2}{\varepsilon\varepsilon_o e N_D}\left(E - E_{fb} - \frac{k_B T}{e}\right) \quad (1)$$

$$\frac{1}{C^2} = \frac{2}{\varepsilon\varepsilon_o e N_D}\left(E - E_{fb} - \frac{k_B T}{e}\right) \quad (2)$$

The exact details of Eq. (1) and (2) and their parameters are published elsewhere [28–36]. The illustration in Fig. 5 is the M–S plots of the passive layers formed on both CG and FG specimens in the test electrolyte.

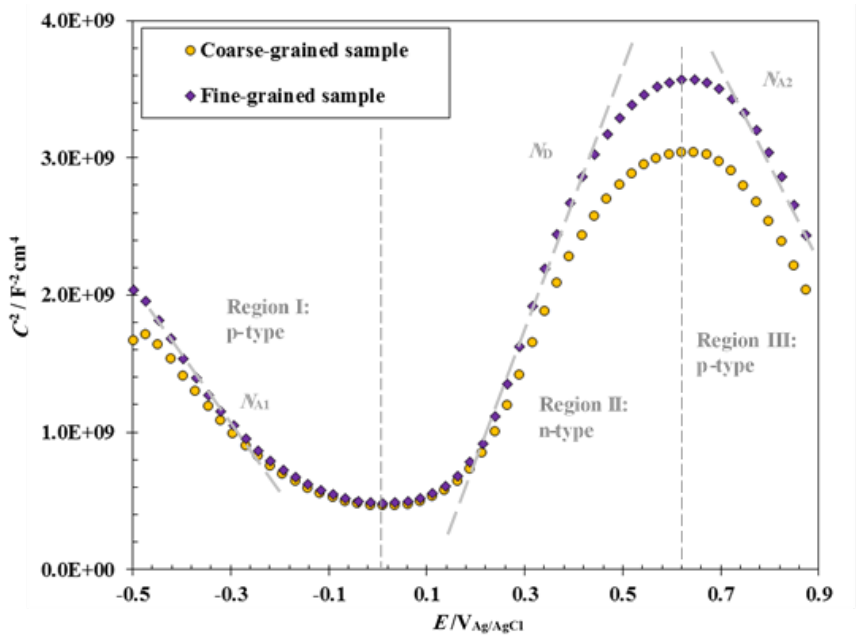

Fig. 5. M–S plots of CG and FG samples in 0.1 M HNO_3 solution

As it is displayed, duplex structure of the formed passive layers and therefore, n- and p-type semiconducting behavior in both specimens are resulted. This is in sensible accordance with the obtained results from previous studies on the other grades of stainless steel in acidic electrolytes [17,28].

Additionally, in both samples, curves are illustrating similar behavior in three distinctive regions. Regions I and III, the negative slopes, are ascribed to the p-type behavior while region II, the positive slope, is indicating the n-type behavior of passive layer [28,29]. Within cathodic region (region I), the presence of Cr_2O_3 in the inner part of the passive layer, results in p-type semiconducting properties [39,40]. In this case, considering Virtanen et al. [41]

survey, p-type semiconductor properties of chromium oxide (Cr_2O_3) in passive layers can be ascribed to the chromium vacancies or excess oxygen. Within the region III, the solid-state oxidation of Cr^{3+} to Cr^{6+} increases the passive layer conductivity and then p-type semiconducting behavior appears. Moreover, the generation of cation vacancies at the interface of passive layer/electrolyte can be the reason of the described semiconducting behavior, either [17,42]. About the bulk metal oxides like Fe_2O_3, M–S plots exhibit no linearity breakdown and consequently, the n-type behavior is because of the Fe^{2+} ions existence as donors [43]. The issue of how two slopes appear in diagrams in anodic domain relating to the passive layers formed on stainless steels, needs yet to be discussed [40,44]. It is reported that the first and second slopes are related to Fe^{2+}, located in tetrahedral and octahedral sites, respectively [45]. In the research of Sikora et al. [44], same levels of oxygen vacancies and Fe^{2+} in octahedral sites are reported. Eq. (1) and (2) represent donor and acceptor densities, concluded from the positive and negative slopes. Fig. 6 demonstrates the donors and acceptor densities (N_{A1} and N_{A2}) for the passive layers of both CG and FG specimens in 0.1 M HNO_3 electrolyte. The value orders are around 10^{21} cm^{-3} and similar to those reported for other stainless steels in acidic environments [17,28]. Fig. 6 reveals reduced quantities of donor and acceptor densities of the FG specimen compared to the CG one. This is the reason for improvement of passive response of the FG specimen. In other words, we have reduced point defects throughout the passive film of the FG specimen whereas the CG samples have a highly defective passive layer on top.

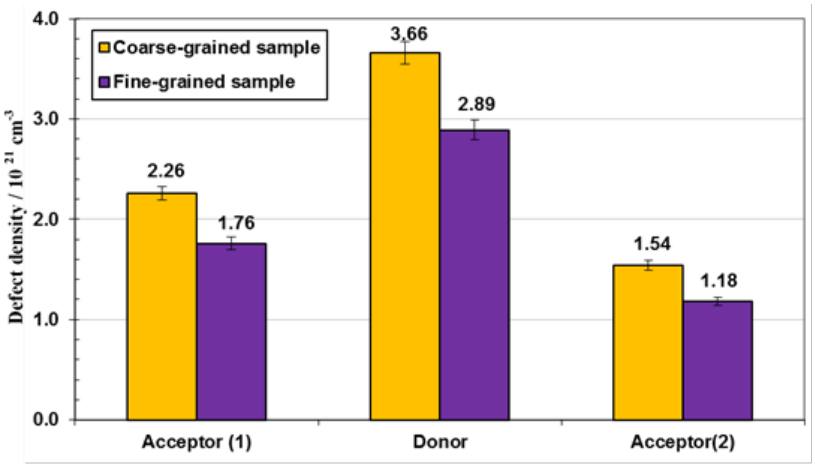

Fig. 6. Changes in the donor and acceptor densities (N_D and N_A) of CG and FG specimens in 0.1 M HNO_3 solution

The achieved results above prove that the defect densities can be affected by the grain size (reduced donor and acceptor densities are obtained by grain refinement process). Accordingly, when the grain refinement process is utilized, the formed passive layers are denser than the passive layers formed on CG specimens.

3.5. EIS measurements

In both CG and FG specimens, the EIS technique was conducted at OCP condition. The responses are demonstrated as Nyquist, Bode, and Bode-phase plots in Fig. 7. A resistive response at high frequencies is recognizable in the Nyquist, Bode and Bode-phase plots.

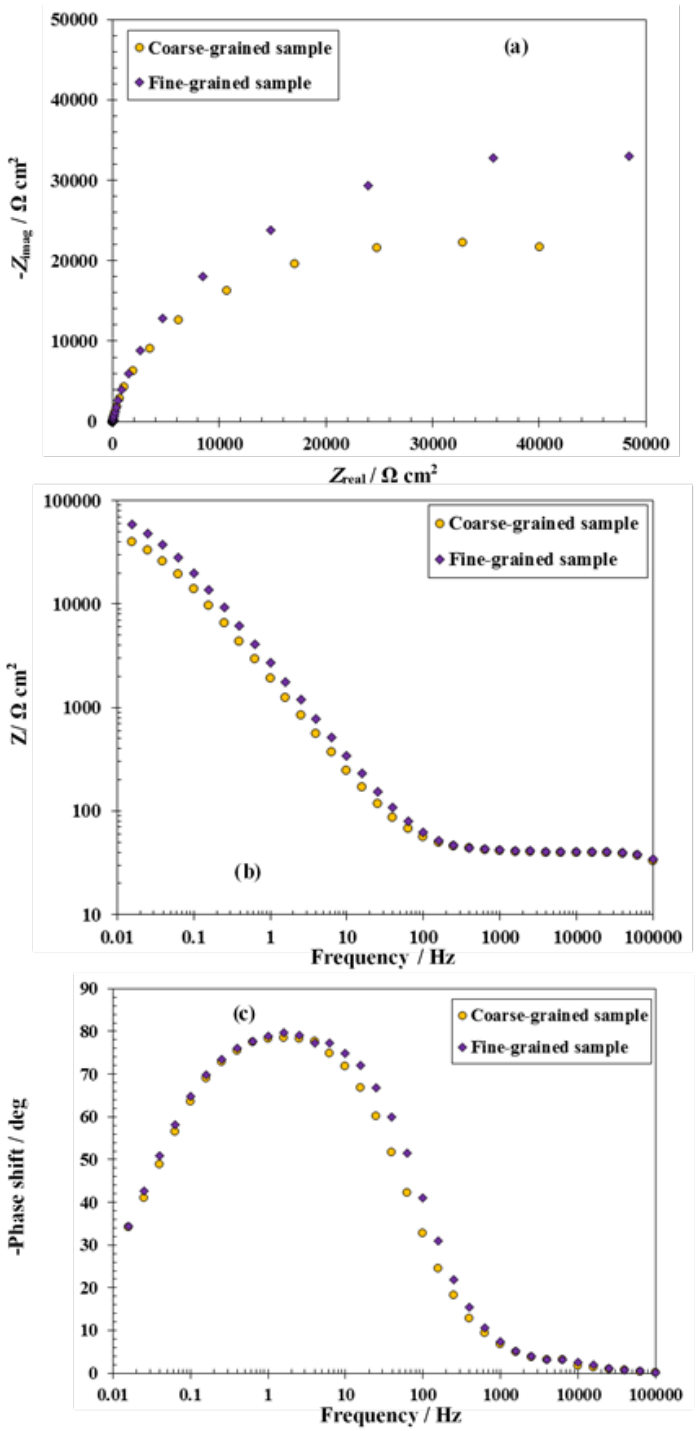

Fig. 7. EIS plots of CG and FG specimens at OCP: (a) Nyquist; (b) Bode and (c) Bode-phase plots

Table 2. Variations in the impedance parameters of coarse-grained and fine-grained samples

	Coarse-grained sample	**Fine-grained sample**
R_S (Ω cm^2)	40.46	40.48
R_{pf} (kΩ cm^2)	52.37	77.82
Y_0 (μF cm^{-2} s^{n-1})	102.1	71.5
n	0.894	0.901

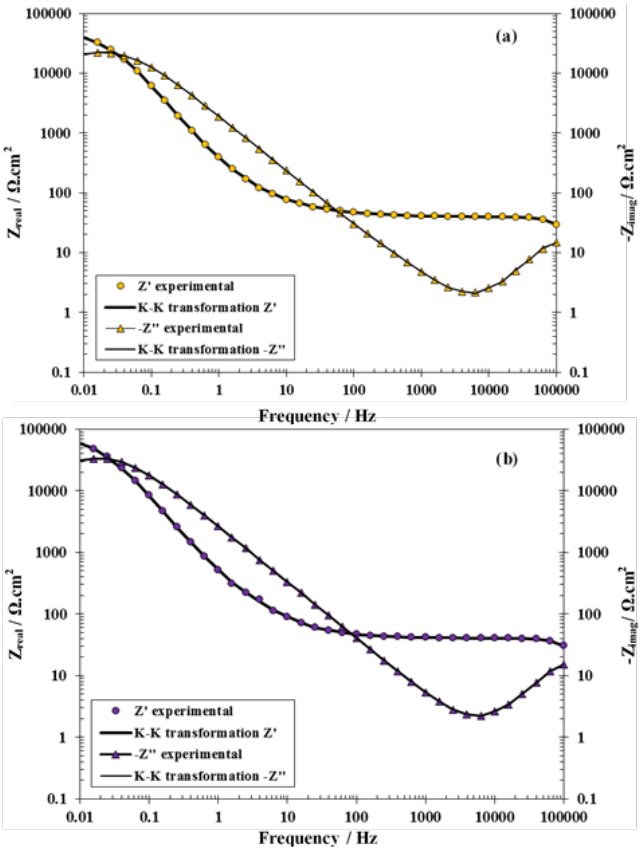

Fig. 8. K–K plots for (a) CG and (b) FG specimens after 1800 seconds of stabilization in 0.1 M HNO_3 solution

According to the forenamed graphs, in the middle to low frequency range there is a distinct capacitive response. Imperfect semicircles are shown in both Nyquist plots. For FG specimen, the semi-circle diameter is higher than its CG counterpart which means grain refinement has bettered the passive response. The Bode-phase curves shown in Fig. 7c, denotes onetime constant. Furthermore, the phase angles values expressed the passive layer formation and growth. To validate the impedance data, the appropriate electrochemical system should comply with the requirements to resolve the linear system constraints theory.

Kramers-Kronig (K–K) transforms are used to confirm the experimental impedance data. Further explanations about K–K formulations can be found elsewhere [46–48]. Drawn comparison between the EIS data and obtained information through the K–K transforms for CG and FG 304 SS specimens in 0.1 M HNO_3 solution is accessible in Fig. 8. As can be observed, the experimental data and the corresponding K–K plots are in good accordance. In order to simulate the impedance data, the electrical equivalent circuit (EEC) shown in Fig. 9 was used [36]. In this EEC, Q_{pf} stands for the constant phase element corresponding to the capacitance of the passive film, R_{pf} is the passive film resistance, and R_S represents the solution resistance. The changes of the EIS parameters of CG and FG specimens in 0.1 M HNO_3 electrolyte are displayed in Table 2.

It is understood that the passive film resistance (R_{pf}) of the FG specimen is higher than that of the CG specimen. Then, it can be inferred that the grain refinement improves the passive layer corrosion resistance. In better words, grain refinement provides more suitable conditions for the passive layer to be created and consequently, improved protective response. Actually, FG specimen is supplied with a great fraction of grain boundaries due to the grain refinement. It should also be mentioned that the advanced corrosion resistance of FG stainless steel is because of the passive layer enriched with more diffusion paths (grain boundaries) [34,36]. Indeed, grain refinement process decreases chromium diffusion free energy. This facilitates the chromium oxide formation and finally the corrosion resistance of FG stainless steel improves considerably. Additionally, in acidic electrolyte, iron dissolution from the top of the layer increases the surface Cr/Fe ratio and also fortifies the chromium rich passive layer. This phenomenon is increased by grain refinement and therefore, the passive layer formation is accelerated [28,49,50].

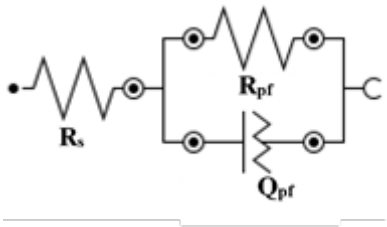

Fig. 9. Best EEC applied to model the EIS data [36]

4. CONCLUSION

Grain refinement impacts on the passive and semiconducting response of 304 SS in 0.1 M HNO_3 electrolyte were evaluated by PDP, M–S and EIS tests. Microstructural observations depicted that reduction in the grain size from about 37 µm to about 380 nm by a factor of ~100 was obtained by thermomechanical operation. PDP plots showed that grain refinement treatment declined both the passive and corrosion current densities. EIS plots demonstrated that implementing the thermomechanical process leads to the higher passive film resistance.

M–S analysis proved that grain refinement does not alter the type of semiconducting behavior (n- and p-type semiconductors) of the passive layers. This test also depicted that the acceptor and donor densities (NA and ND) are in the range of 1021 cm-3 and dropped with grain refinement. All results revealed that grain refinement in micro-scales enhances the electrochemical corrosion behavior of 304 SS. These results pointed out the formation of more stable and compact passive layer through the refinement of microstructure.

REFERENCES

[1] H. Halfa, JMMCE 2 (2014) 428.
[2] S. Vafaeian, A. Fattah-alhosseini, Y. Mazaheri, and M. K. Keshavarz, Mater. Sci. Eng. A 669 (2016) 480.
[3] Y. Zhu, R. Z. Valiev, T. G. Langdon, N. Tsuji, and K. Lu, MRS bulletin 35 (2010) 977.
[4] B. Ravi Kumar, R. Singh, B. Mahato, P. K. De, N. R. Bandyopadhyay, and D. K. Bhattacharya, Mater. Charact. 54 (2005) 141.
[5] Y. Estrin, and A. Vinogradov, Acta Mater. 61 (2013) 782.
[6] S. Miran, IJMSCI 4 (2014) 98.
[7] S. Bagherifard, R. Ghelichi, A. Khademhosseini, and M. Guagliano, ACS Appl. Mater. Interfaces 6 (2014) 7963.
[8] M. Moallemi, A. Najafizadeh, A. Kermanpur, and A. Rezaee, Mater. Sci. Eng. A 530 (2011) 378.
[9] M. Eskandari, A. Najafizadeh, A. Kermanpur, and M. Karimi, Mater. Des. 30 (2009) 3869.
[10] F. Forouzan, A. Najafizadeh, A. Kermanpur, A. Hedayati, and R. Surkialiabad, Mater. Sci. Eng. A 527 (2010) 7334.
[11] T. Roland, D. Retraint, K. Lu, and J. Lu, Mater. Sci. Eng. A 445–446 (2007) 281.
[12] S. V. Dobatkin, O. V. Rybal'chenko, and G. I. Raab, Mater. Sci. Eng. A 463 (2007) 41.
[13] A. Di Schino, and J. Kenny, J. Mater. Sci. Lett. 21 (2002) 1969.
[14] Z.W. Wu, J. Chen, N. Piao, C. Sun, W. Hassan, X. H. Zhang, Y. J. Xie, and T. Nonferr. Metal. Soc. 24 (2014) 1989.
[15] L. Jinlong, and L. Hongyun, J. Mater. Eng. Perform. 23 (2014) 4223.
[16] Z.J. Zheng, Y. Gao, Y. Gui, and M. Zhu, Corros. Sci. 54 (2012) 60.
[17] A. Fattah-alhosseini, and S. Vafaeian, Appl. Surf. Sci. 360 (2016) 921.
[18] S. Vafaeian, A. Fattah-alhosseini, M. K. Keshavarz, and Y. Mazaheri, J. Alloys Compd. 677 (2016) 42.
[19] H. Wang, and J. A. Turner, J. Power Sources 128 (2004) 193.
[20] Z. J. Zheng, Y. Gao, Y. Gui, and M. Zhu, Corros. Sci. 54 (2012) 60.
[21] X. Q. Cheng, C. F. Dong, X. G. Li, and W. D. Li, Mater. Res. Innovations 17 (2013)557.

[22] J. Yang, Q. Wang, and K. Guan, Int. J. Pressure Vessels Piping 110 (2013) 72.
[23] L. Wang, B. Kang, N. Gao, X. Du, L. Jia, and J. Sun, J. Power Sources 253 (2014) 332.
[24] V. S. Moura, L. D. Lima, J. M. Pardal, A. Y. Kina, R. R. A. Corte, and S. S. M. Tavares, Mater. Charact. 59 (2008) 1127
[25] C. T. Kwok, F. T. Cheng, H. C. Man, and W. H. Ding, Mater. Lett. 60 (2006) 2419.
[26] J. A. Bardwell, G. I. Sproule, B. MacDougall, M. J. Graham, A. J. Davenport, and H. S. Isaacs, J. Electrochem. Soc. 139 (1992) 371.
[27] W. S. Tait, An introduction to electrochemical corrosion testing for practicing engineers and scientists. USA: PairODocs Publications (1994).
[28] A. Fattah-alhosseini, Arab. J. Chem. 9 (2016) S1342.
[29] A. Fattah-alhosseini, A. Moradi, E. Moradi, and N. Attarzadeh, Anal. Bioanal. Electrochem. 6 (2014) 284.
[30] Y. Zhang, M. Urquidi-Macdonald, G. R. Engelhardt, and D. D. Macdonald, Electrochim. Acta 69 (2012) 1.
[31] S. Yang, and D. D. Macdonald, Electrochim. Acta 52 (2007) 1871.
[32] M. J. Carmezim, A. M. Simões, M. F. Montemor, and M. D. Cunha Belo, Corros. Sci. 47 (2005) 581.
[33] H. Luo, C. F. Dong, K. Xiao, and X. G. Li, Appl. Surf. Sci. 258 (2011) 631.
[34] L. Jinlong, and L. Hongyun, Appl. Surf. Sci. 280 (2013) 124.
[35] L. V. Jin-long, and L. Hong-yun, Mater. Chem. Phys. 135 (2012) 973.
[36] S. Vafaeian, A. Fattah-alhosseini, M. K. Keshavarz, and Y. Mazaheri, J. Mater. Eng. Perform. 26 (2017) 676.
[37] J. Amri, T. Souier, B. Malki, and B. Baroux, Corros. Sci. 50 (2008) 431.
[38] L. Jinlong, and L. Hongyun, Appl. Surf. Sci. 263 (2012) 29.
[39] N. B. Hakiki, S. Boudin, B. Rondot, and M. Da Cunha Belo, Corros. Sci. 37 (1995) 1809.
[40] F. Gaben, B. Vuillemin, and R. Oltra, J. Electrochem. Soc. 151 (2004) B595.
[41] S. Virtanen, P. Schmuki, H. Bohni, P. Vuoristo, and T. Mantyla, J. Electrochem. Soc. 142 (1995) 3067.
[42] T. L. S. Wijesinghe, and D. J. Blackwood, J. Electrochem. Soc. 154 (2007) C16.
[43] P. Schmuki, M. Buchler, S. Virtanen, H. Bohni, R. Muller, and L. J. Gauckler, J. Electrochem. Soc. 142 (1995) 3336.
[44] E. Sikora, and D. D. Macdonald, J. Electrochem. Soc. 147 (2000) 4087.
[45] N. E. Hakiki, M. Da Cunha Belo, A. M. P. Simões, and M. G. S. Ferreira, J. Electrochem. Soc. 145 (1998) 3821.
[46] M. Schönleber, D. Klotz, and E. Ivers-Tiffée, Electrochim. Acta 131 (2014) 20.
[47] B. A. Boukamp, Solid State Ionics 62 (1993) 131.

[48] S. Fajardo, D. M. Bastidas, M. Criado, and J. M. Bastidas, Electrochim. Acta 129 (2014) 160.
[49] G. T. Burstein, and P. I. Marshall, Corros. Sci. 24 (1984) 449.
[50] M. A. Barbosa, A. Garrido, A. Campilho, and I. Sutherland, Corros. Sci. 32 (1991) 179.